Pathophysiology Aspects of Muscle Atrophy and Osteopenia Induced by Chronic Constriction Injury (CCI) of the Sciatic Nerve in Rat

Francesca Bosco
University Magna Graecia of Catanzaro
Lorenza Guarnieri
University Magna Graecia of Catanzaro
Saverio Nucera
University Magna Graecia of Catanzaro
Miriam Scicchitano
University Magna Graecia of Catanzaro
Stefano Ruga
University Magna Graecia of Catanzaro
Antonio Cardamone
University Magna Graecia of Catanzaro
Samantha Maurotti
University Magna Grecia
Cristina Russo
University Magna Grecia
Anna Rita Coppoletta
University Magna Graecia of Catanzaro
Roberta Macrì
University Magna Graecia of Catanzaro
Irene Bava
University Magna Graecia of Catanzaro
Federica Scarano
University Magna Graecia of Catanzaro
Fabio Castagna
University Magna Graecia of Catanzaro
Maria Serra
University Magna Graecia of Catanzaro
Rosamaria Caminiti
University Magna Graecia of Catanzaro
Jessica Maiuolo

University Magna Graecia of Catanzaro
Sara Ilari
University Magna Graecia of Catanzaro
Filomena Lauro
Saint Louis University School of Medicine
Luigino Antonio Giancotti
Saint Louis University School of Medicine
Carolina Muscoli
University Magna Graecia of Catanzaro
Cristina Carresi
University Magna Graecia of Catanzaro
Ernesto Palma
University Magna Graecia of Catanzaro
Micaela Gliozzi (gliozzi@unicz.it)
University Magna Graecia of Catanzaro
Vincenzo Musolino
University Magna Graecia of Catanzaro
Vincenzo Mollace
University Magna Graecia of Catanzaro

Research Article

Keywords: Chronic Constriction Injury, Muscle atrophy, Muscle atrophy model, Osteoporosis, Osteopenia, Osteosarcopenia.

Posted Date: March 24th, 2022

DOI: https://doi.org/10.21203/rs.3.rs-1463017/v1

Abstract

Background

Skeletal muscle atrophy is a condition characterized by a loss of muscle mass and muscle strength. This condition correlates with an imbalance between protein synthesis and protein degradation caused by the hyperactivation of some cellular catabolic pathways. Muscle and bone interact through physical forces and chemical pathways and muscle atrophy is often associated with a loss of bone mass manifesting as osteoporosis. The aim of this study was to evaluate if Chronic Constriction Injury (CCI) of sciatic nerve can be a valid model to study muscle atrophy and consequent osteoporosis.

Methods

In this study the effects of CCI performed on sciatic nerve were tested in rat. Body weight and body composition were assessed at baseline and once per week till the end of the study. Magnetic resonance imaging (MRI) was performed at day zero before ligation and at day 28 before sacrifice. On gastrocnemius muscles catabolic markers were assessed by western blot analysis and a morphological analysis of cross-sectional area of muscle fibers was performed by hematoxylin and eosin staining. After the sacrifice a Micro-Computed Tomography (Micro-CT) on the tibia bone was performed and bone calcium content was determined. Quantitative Real Time PCR was performed on both bone and muscle tissue to quantify expression levels of genes involved in osteopenia and muscle atrophy.

Results

Rats underwent to CCI had a lower body weight increase at day 28 compared to the naive group of rats ($p < 0.001$). The increase in lean body mass and fat mass was also significantly lower in CCI group, compared with the non-operated control rats ($p < 0.001$). The weights of the skeletal muscle were significantly lower in the ipsilateral hindlimb compared to contralateral muscles; furthermore, the cross-sectional area of muscle fibers decreased significantly in the ipsilateral gastrocnemius. The CCI of the sciatic nerve induced a statistically significant increase of Autophagic and UPS markers protein expression and mRNA expression levels of fbx32 and of TRAF-6 resulted also higher in ipsilateral gastrocnemius. Western blotting analysis showed a statistically significant increase of Pax-7 expression in the ipsilateral GC of rats 28 days after surgery, compared to the contralateral gastrocnemius muscle. Micro-CT showed a statistically significant decrease in the parameters of bone mineral density, bone volume fraction, bone surface density, trabecular number, connectivity density, and bone perimeter of the tibial bone on the ipsilateral hindlimb rather than contralateral tibial bone, whereas the structure model index was significantly higher at 28 days after the surgery. Gene expression levels of TRAF-6 resulted significantly up-regulated in ipsilateral femur.

Conclusions

In this study, chronic nerve constriction appeared to be a valid model for inducing the condition of muscle atrophy causing also changes in bone microstructure and leading to osteoporosis. Therefore, sciatic

nerve constriction could be a valid approach to study the muscle-bone crosstalk, and to identify new strategies to prevent osteosarcopenia.

Introduction

Skeletal muscle is one of the largest tissues in the human body and it is fundamental to the generation of force and in locomotion. The high plasticity of muscle tissue is due to its ability of both structural and functional adaptation to external stimuli, which is responsible for changes in muscle mass [1]. The lack of muscle mass and strength is associated with reduced quality of life, independence, and life expectancy. Muscle loss is a condition associated with many diseases such as heart failure, cancer, Chronic obstructive pulmonary disease (COPD), diabetes, AIDS [2, 3, 4]. Furthermore, muscle atrophy is often associated with osteoporosis, a bone tissue disorder characterized by bone density and strength reduction. The co-existence of osteoporosis and muscle loss leads to the definition of the "osteosarcopenia syndrome" with an increasing risk of bone fracture, consequent hospitalization, immobilization, and a reduction of quality of life [5]. Since there are no specific drugs for the treatment of this syndrome, the only therapeutic approach is mainly based on the dietary supplementation accompanied by physical activity to increase the trophic stimulus on the musculoskeletal system [6, 7]. However, in many situations, i.e., critically ill patients, fractures, or nerve damage, patients are unable to perform physical activity and immobility makes this remedy ineffective or otherwise inapplicable [8]. Although peripheral nerve damage is a clinical condition that might be caused by disease [9], physical trauma is the most common cause of injury to the nerves [10, 11]. A widely animal model used to study peripheral nerve damage provides a chronic constriction injury to the sciatic nerve [12] and it is accompanied by symptoms such as neuropathic pain, motor dysfunction and skeletal muscle atrophy [12, 13, 14, 15]. Although Chronic Constriction Injury (CCI) is a well investigated model for research of neuropathic pain in animals, very little is known about the musculoskeletal changes associated with this injury.

The muscle tissue healthy is guaranteed by the balance between protein synthesis and degradation [16, 17, 18]. Generally, loss of muscle mass can be because of a decreased rate of protein synthesis, an increased rate of protein degradation or both [19]. Increased protein degradation in atrophic muscle appears to be linked to an increased activity of two major protein degradation pathways, the autophagic pathway and the ubiquitin-proteasome system (UPS) [15, 20, 21]. These pathways involve several atrogenes, which could activate the muscle wasting program in many conditions, such as starvation, cancer cachexia, denervation, heart failure and aging [22, 23].

However, in CCI-induced muscle atrophy, while the catabolic machinery is activated, protein synthesis rates are increased during nerve damage induced muscle loss, suggesting a compensatory mechanism of muscle remodelling [13, 14]. Contextually, in this scenario, regeneration ability mediated by the muscle-specific stem cells, are not guaranteed and satellite cells remain in the quiescent phase without the possibility of differentiating into myoblasts [24, 25, 26]. Furthermore, bone loss has been recognized in connection with muscle disuse and dysfunction [27], but also because of nerve damage induced by crush

[28] or loose constriction of the sciatic nerve [29], which could lead to a change in bone mineral content (BMC) and bone mineral density (BMD) [29, 30]. Although it is possible that nerve injury causes a direct alteration in bone–nerve interaction and a loss of BMD, it is not easy to give a clear proof to the direct effects of nerve injury on BMD as constriction of the sciatic nerve causes immobilization, paralysis, and a reduction in mechanical loading, which in turn reduces BMD.

In the present study, we hypothesized that CCI of the sciatic nerve causes an effect on body weight and body composition over 28 days and exerts a modulation of the catabolic pathways in the gastrocnemius (GC) muscle. Furthermore, we also hypothesized a modification of the microstructure of the tibial bone following damage to the sciatic nerve.

Methods

Animals

Adult male Wistar Han rats (n = 58) weighing 250 g ± 4g were randomly divided into two groups: the naïve group (n = 10) and the CCI group (n = 48). At day 0, sciatic nerve ligation was performed on the right hindlimb of all the rats belonging to the CCI group. The left (contralateral) hindlimb was operated but without ligation of the sciatic nerve.

One day before the surgery, baseline body weight and body composition were assessed. The same parameters were assessed once per week till the end of the study.

Magnetic resonance imaging (MRI) was performed at day zero before ligation and at day 28 before sacrifice. The day of sacrifice, animals were anesthetized and euthanized, and muscles were rapidly removed, weighed, and immediately frozen in liquid nitrogen or fixed in 10% formalin for further analysis. After the sacrifice a Micro-computed tomography on tibias was performed.

All the experimental procedures conduced on animals were performed according to protocols approved by the Animal Care of University Magna Graecia of Catanzaro and were carried out in compliance with the ARRIVE guidelines. All experiments were performed in accordance with the European Commission guidelines (Directive 2010/63/EU) for the animals used for scientific purposes.

Chronic Constriction Injury (CCI)

The surgery was performed under anesthesia, induced with 5% isoflurane in oxygen and then maintained with 2% isoflurane in oxygen. Anesthetized animals were monitored constantly during the surgery. On the right hindlimbs (ipsilateral), the sciatic nerve was exposed by making a skin incision, and cutting through the connective tissue, 3–4 mm below the femur, between the gluteus superficialis and biceps femoral muscle. Four loosely constrictive ligatures of 4.0 chromic gut were tied around the right sciatic nerve with a double knot, 1 mm apart, proximal to the trifurcation of the sciatic nerve, to occlude, but not arrest

epineural blood flow. An identical surgery, without sciatic nerve damage, was performed in the left hindlimb (contralateral). Staples were used to suture (Autoclip, 9 mm) and the wounds were disinfected using an iodine solution (Riodine). After the surgery, the rats were housed individually in cages [12].

Body composition analysis

Total body fat, lean mass, and body fluids were measured using a nuclear magnetic resonance spectroscopy device EchoMRI-700TM (Echo Medical System, Houston, TX, USA), as previously described [31].

Magnetic resonance imaging

Before magnetic resonance imaging, rats were anaesthetized with 4% isoflurane (Forane, Abbott) vaporized in oxygen (flow: 2 l/min) and then kept during the acquisition between 2 and 3% to maintain the breathing rhythm between 40 and 60 breaths per minute. All the vital parameters were monitored, through a multiparametric monitor. The body temperature was maintained at 37°C. MRI images were acquired with a Bruker Pharmascan 70/16 US 7 Tesla bore MR scanner (Bruker Biospin MRI GmbH, Ettlingen, Germany), equipped with a total body transmitter receiver coil. Axial T2_turboRARE weighted images with fat suppression were acquired with the following parameters: relaxation time (TR) 800.000 ms, echo time (TE) 25.00 ms, averages 8, slices 9, thickness of 1 mm, repetitions 1, field of view 58x58 mm^2.

Muscle segmentation

Manual segmentation was performed using OsiriX imaging software (v. 12.0.2, Pixmeo SARL, Switzerland). The margins of individual muscle in Axial T2_turboRARE weighted images were manually traced through the "Draw tool" as defined in Greene's Rat Anatomy Atlas [32], and in a more recently experiment performed by Zhang et al. [33]. The slice used is the same for all animals and it represents the exact distance from epiphysis and diaphysis. To improve the viewing of individual muscle margins, a Default WL / WW, "Vr Muscles-Bones Clut" and a Logarithmic opacity table were used.

Protein extraction and western blot

50mg of GC muscle were homogenized in 500μL ice-cold lysis buffer (20mM Tris–HCl pH 7.5; 150mM NaCl; 1mM EDTA; 1mM EGTA; 1% 43 Triton X-100; 2,5mM Na4P2O7; 20mM NaF; 1mM dithiothreitol; 1mM Na3VO4; 1mM β-glycerophosphate; and 10 μL/mL freshly added protease and phosphatase inhibitor cocktails), centrifuged at 14000×g for 20min at 4°C and supernatant was collected. A total of 20μL of the supernatant was used to determine the total protein concentration with a Bradford assay (Bio-Rad, Hercules, California, USA) using bovine serum albumin as a standard. Proteins were heat

denatured for 5min at 95°C in sample loading buffer (500mM Tris/HCl, pH 6.8; 30% Glycerol; 10% sodium dodecyl sulfate; 5% β-mercaptoethanol; and 0,024% bromophenol blue), and 30µg of protein lysate was resolved by sodium dodecyl sulfate polyacrylamide gel electrophoresis and transferred to nitrocellulose membranes (GE Healthcare,10600001). After incubation in a blocking solution (5% dry non-fat milk, Sigma-Aldrich, St. Louis, MO), membranes were incubated overnight at 4°C shaking with the following primary antibodies: Beclin-1 (3738, Cell Signaling Technology, Boston, USA), LC3-II/LC3-I (PM-036, MBL, Woburn, USA), p62 (M162-3, MBL, Woburn, USA), TRAF-6 (Ab 33915, Abcam, Cambridge, UK), Atrogin-1 (ab168372, Abcam, Cambridge, UK), Pax-7 (MABD20 Merk Millipore, Darmstadt Germania) and GAPDH (ab181602, Abcam, Cambridge, UK); all antibodies were used at 1:1000 concentration. Membranes were then washed in TBS (pH 7.6) with 0.1% Tween-20 and incubated with a secondary antibody for 1h at RT with shaking [20].

Histological analysis

GC muscles of rats were harvested and fixed in 10% formalin for 24 hours and paraffin embedded for morphological analysis of cross-sectional area of muscle fibers. For the assessment of tissue morphology, 5-µm-thick sections of muscles were stained H&E and visualized at room temperature on a microscope (Olympus bx53, U-LH100HG) using a digital camera (Nikon) at 20X magnification, and Olympus cellSens Dimension 1.1 Software. The images, stored as JPEG files, were equally adjusted using Photoshop CS2 software (Adobe). For each muscle, the distribution of fiber CSA was calculated by analyzing 400 myofibers.

Micro-Computed Tomography

After the sacrifice, the tibias were explanted from the animal, and stored in alcohol at a temperature of 4°C. Right and left tibias were scanned using a SkyScan 1176 (SkyScan, Kontich, Belgium). The explanted bones were removed from alcohol storage and dried superficially on paper tissue, before being wrapped in plastic “cling-film” or in parafilm, to prevent drying during scanning (and associated movement artefacts). Each plastic-wrapped bone was placed in a plastic/polystyrene foam tube which was mounted horizontally in the 1176 scanner sample chamber, for micro-CT imaging. Reconstruction was carried out using the Skyscan Nrecon2 software which facilitates network distributed reconstruction carried out on four pcs running simultaneously. The time needed for the reconstruction of the dataset scan is usually much less than the scan duration.

Trabecular bone was assessed in 400 slices of proximal tibia (immediately distal to the epiphyseal plate). Settings were Source Voltage 65 KVp, Source Current 380 µA. Trabecular bone was manually segmented. Parameters are reported according to published guidelines. Trabecular parameters included bone volume fraction (BV/TV), number (Tb.N), thickness (Tb.Th), separation (Tb.Sp), structure model index (SMI), connectivity density (Conn.D) [34].

Bone calcium content

Right and left tibias were isolated and cleaned of soft tissue. The bones were dried at 110°C for 6 hours and weighed, then were ashed at 800°C for 4 hours, weighed again and dissolved in 1mL 6N HCl. Calcium content was determined by colorimetric determination with Quantichrom calcium Assay kit (BioAssay Systems, Hayward, CA).

Reverse Transcription and Quantitative Real Time PCR (qRT-PCR) performed on GC muscle tissue

Total RNA from GC muscle was extracted with Trizol reagent (Gibco, Life Technologies, Carlsbad, CA, USA) according to manufacturer's instructions. The RNA quantity and quality were assessed through NanoDrop® ND-2000 Spectrophotometer (Waltham, MA, USA). To evaluate transcript changes, 1000 ng of total RNA was reverse-transcribed to cDNA using the "High Capacity cDNA Reverse Transcription Kit" (Applied Biosystems, Carlsbad, CA, USA).

The following TaqMan gene expression assays (Applied Biosystems, Carlsbad, CA, USA) were used to detect and quantify genes using the Viia7 DX real time PCR instrument (Life Technologies, Waltham, MA, USA): TRAF-6 (Rn00590197_m1), Atrogin-1 (fbx32) (Rn00591730_m1), and GAPDH (Rn01462661_g1).

Reverse Transcription and Quantitative Real Time PCR (qRT-PCR) performed on femurs bone

The rat femurs were homogenized using gentleMACS Dissociators (Miltenyi). Total RNA from femurs were extracted with Trizol reagent (Gibco, Life Technologies, Carlsbad, CA, USA) according to manufacturer's instructions.

The RNA quantity and quality were assessed through NanoDrop® ND-2000 Spectrophotometer (Waltham, MA, USA). To evaluate transcript changes, 1000 ng of total RNA was reverse transcribed to cDNA using the "High-Capacity cDNA Reverse Transcription Kit" (Applied Biosystems, Carlsbad, CA, USA). mRNA expression of TRAF-6, alkaline phosphatase (ALP), RANKL, osteoprotegerin (OPG), RUNX2 and β-ACTIN were quantified by real time-PCR using SYBR® Green dye (SYBR® Green PCR Master Mix, Applied Biosystems, Foster City, CA, USA) (see Table 1).

Table 1. Primers of genes used for real-time PCR on femurs bone.

Gene	Forward primer	Reverse primer	Ref. gene
RANKL	ACTTTCGAGCGCAGATGGAT	GCCTGAAGCAAATGTTGGCG	NM_057149.1
OPG	CCCAACGTTCAACAACCCAA	GGGCGCATAGTCAGTAGACA	NM_012870.2
RUNX2	CACAAGTGCGGTGCAAACTT	TGAAACTCTTGCCTCGTCCG	NM_001278483.1
ALP	TTGCTAGTGGAAGGAGGCAG	CATTGTGGGCTCTTGTGGGA	NM_013059.2
TRAF-6	ACTTGATCTCGGAGTGCTGC	CGTGACAGCCAAACACACTG	NM_001107754.2
β-ACTIN	CCGCGAGTACAACCTTCTTG	CGTCATCCATGGCGAACTGG	NM_031144.3

Real-time PCR data analysis

To carry out the analysis of data obtained by real-time PCR, the arithmetic mean of the Ct (Threshold Cycle) in triplicate values was performed. ΔCt was calculated as the difference between Ct of the refence gene and Ct of the target gene. ΔΔCt was calculated as the difference between the mean of the ipsilateral ΔCt and the mean of the contralateral ΔCt. The statistical significance was calculated on the ΔCt values [35].

Statistical analysis

The data were analyzed with GraphPad PRISM 9.1.2 (Graph Pad Software, Inc., La Jolla, CA, USA). All data were expressed as mean ± S.E.M. Normally distributed data of body weight and body composition were analyzed by one way ANOVA, followed by the Tukey's test, while data not normally distributed were analyzed using Kruskal–Wallis analysis of variance, followed by Dunn's tests. The Unpaired Two-tailed Student's t-test was used for statistical analysis of data of muscle weight, Cross sectional area of fibers, western blotting analysis, and bone parameters. PCR data was tested by a Student's t-test and 95% confidence interval (CI). Values with $p < 0.05$ were considered statistically significant.

Results

Body weight and body composition of rats underwent chronic constriction injury

Rats underwent CCI had a lower body weight increase at day 28 compared to the naive group of rats ($p<0.001$; Figure1A)

The increase in lean body mass and fat mass was significantly lower in CCI group, compared with the non-operated control rats ($p<0.001$; Figure 1B,C).

Constriction injury of the sciatic nerve induces muscle wasting in rats

The CCI of the sciatic nerve had strong effects on the individual muscles. The weights of soleus muscle, extensor digitalis longus muscle (EDL), and tibialis muscle were significantly lower in the hindlimb compared with contralateral muscles (Figure 2).

Moreover, ipsilateral GC muscle weight is lower compared to the contralateral muscle 28 days after CCI (Figure 3E). Sciatic nerve damage leads to a fully developed muscle wasting phenotype at 28 days post-surgery (Figure 3A,B; Figure 4; Figure 5). Interestingly the cross-sectional area (CSA) of muscle fibers visualized by haematoxylin and eosin (H&E) staining (Figure 3C,D) decreased significantly in the ipsilateral GC compared to the contralateral side (Figure 3F).

Catabolic pathways in rat gastrocnemius muscle after chronic sciatic nerve constriction injury

The CCI of the sciatic nerve induced a statistically significant increase of Beclin-1 expression (Figure 6A).

A significant increase of microtubule-associated protein 1 light chain 3B isoform I (LC3B-I) was detected (Figure 6B). Moreover, the levels of p62, a marker of substrate sequestration into autophagosome, was assayed. Levels of p62 were significantly higher in the injured ipsilateral skeletal muscle GC than in those of the contralateral side (Figure 6C). In addition, levels of the protein TRAF-6 were higher in the ipsilateral GC than in the contralateral muscle (Figure 6D). Interestingly, the Ubiquitin-protein ligase, Atrogin-1, was significantly up-regulated (Figure 6E). Western blotting analysis showed that CCI of the sciatic nerve induced also a statistically significant increase of Pax-7 expression in the ipsilateral GC of rats 28 days after surgery, compared to the contralateral GC muscle (Figure 6F).

E3 ubiquitin ligases gene expression analysis in gastrocnemius muscle after CCI of sciatic nerve

Considering the up regulation of fbx32 and TRAF-6 proteins in the GC muscle, we also evaluated the gene expression levels of these two ubiquitins. As shown in Figure 7, also mRNA expression levels of fbx32 and of TRAF-6 resulted higher in ipsilateral GC compared to contralateral muscle (Figure 7; Table 2).

Table 2. Statistical analysis of real-time PCR. Mean ± S.D., the 95% Confidence interval and p-value of both ΔCt and ΔΔCt have been reported.

	ΔCT		ΔΔCT		
	Mean ± SD	95% CI [lower ~ upper]	Mean ± SD	95% CI [lower ~ upper]	P value
fbx32	1.555 ± 1.157	[0.997 ~ 2.112]	1.453 ± 1.157	[0.896 ~ 2.011]	p<0.001
TRAF-6	2.840 ± 1.085	[2.317 ~ 3.363]	1.132 ± 1.085	[0.609 ~ 1.655]	p<0.001

Bone microstructure observation of tibia bone following constriction injury of sciatic nerve

Micro-CT (Figure 8) showed that many parameters, such as bone mineral density (BMD), bone volume fraction (BV/TV), bone surface density (BS/TV), trabecular number (Tb.N), connectivity density, bone perimeter (B.Pm) of the tibial bone on the ipsilateral hindlimb side were significantly lower than the contralateral tibial bone (Figure 9), whereas the structure model index (SMI) was significantly higher at 28 days after the surgery (Figure 9). Moreover, calcium content showed a trend toward a reduction in the tibial bone on the ipsilateral hindlimb when compared to the contralateral side (p=0.0879; Figure 9).

Gene expression analysis in femurs after CCI of sciatic nerve

To investigate the mechanisms by which chronic sciatic nerve constriction and subsequent muscle atrophy are related to bone damage we evaluated the gene expression of TRAF-6, Alkaline Phosphatase, osteoprotegerin (OPG), RANKL, and RUNX2 (Figure 10; Table 3). Gene expression levels of TRAF-6, analyzed by method of ΔCT, resulted significantly up-regulated in ipsilateral femur (Figure 10; Table 3).

Table 3. Statistical analysis of real-time PCR. Mean ± S.D., the 95% Confidence interval and p-value of both ΔCt and ΔΔCt have been reported.

	ΔCT		ΔΔCT		
	Mean ± SD	95% CI [lower ~ upper]	Mean ± SD	95% CI [lower ~ upper]	P value
ALP	-1.435 ± 0.484	[-2.035 ~ -0.834]	0.545 ± 0.4837	[-0.051 ~ 1.150]	ns
OPG	0.2374 ± 1.029	[-1.041 ~ 1.515]	-0.741 ± 1.029	[-2.019 ~ 0.537]	ns
RUNX2	-11.08 ± 1.104	[-12.45 ~ -9.708]	-0.898 ± 1.104	[-2.268 ~ 0.472]	ns
TRAF-6	-3.060 ± 0.749	[-3.990 ~ -2.130]	1.166 ± 0.749	[0.235 ~ 2.097]	p<0.05
RANKL	-11.42 ± 1.549	[-13.89 ~ -8.954]	-1.115 ± 1.548	[-3.579 ~ 1.349]	ns

Discussion

Here, we have demonstrated that (i) CCI injury of the sciatic nerve, performed in young rats, caused a change in overall weight and body composition. (ii) This change was associated with skeletal muscle atrophy of ipsilateral hindlimb driven by an hyperactivation of autophagy and UPS. (iii) The levels of Pax-7 were sustained 28 days after chronic constriction injury, suggesting that differentiation of muscle cells could be impaired by CCI-induced atrophy and wasting. (iv) CCI injury also induces changes in bone microstructure leading to osteoporosis.

Chronic constriction injury (CCI) is a well-known model to study peripheral nerve damage [12, 36, 37] which is accompanied by debilitating symptoms such as neuropathic pain, and hampered motor function, but very little is known about musculoskeletal and osteopathic changes associated with this injury, even though it is a widely used model for neuropathic pain research [38, 39]. In this experiment, the group underwent to ligation of the sciatic nerve had a significant lower body weight, on day 28 of the experiment compared to the control group, which gained less weight than expected, according to guidelines provided by the breeder (Envigo Harlan). Our results are consistent with previous studies which reported that body weight in rats subjected to CCI surgery was less compared to sham groups over a 14-day period [40, 41]. In our study, rats belonging to CCI group, showed atrophy in the muscle innervated by branches of the sciatic nerve [38, 42]. Atrophy-induced by ligation of the sciatic nerve is well documented. Indeed, other groups have reported atrophy of the soleus [13, 40, 43], tibialis and EDL [13], GC and rectus femoris muscles [44, 45] after peripheral nerve injury.

Moreover, the total number of fibers, indicates a reduction in the CSA area in ipsilateral muscle and a subsequent muscular atrophy due to loss of mass in individual fibers, which could be consistent with muscular atrophy rather than dystrophy [46]. Furthermore, the MRI image, also indicates a reduction in mass of the damaged hindlimb, and the manual muscle segmentation showed a reduction of individual ipsilateral muscles volume compared to the contralateral.

Sciatic nerve ligation is a loose ligation that causes epineural swelling and inflammation, but it leaves the axons intact [12, 47, 48], so the amount of muscle denervation occurring in CCI is less than in other more severe injury models such as crush injury [49]. The reduced activity in CCI rats post-surgery suggests that hypokinesia plays a very important role in the muscle atrophy. Earlier studies have shown that muscle atrophy occurs in soleus, EDL, GC, and tibialis muscles with cast immobilization in mice [50] as well as with tail cast suspension [51], space flight, and whole-body suspension in rats [52], as well as in sciatic injured models [53]. Generally, loss of muscle mass can be due to a decreased rate of protein synthesis, an increased rate of protein degradation or both. There is a consensus that in many chronic diseases, such as cachexia, COPD, or heart failure, atrophy is caused by a sustained proteolysis. Although in disuse atrophy and immobilization in humans, a decrease in myofibrillar protein synthesis appears to be the predominant mechanism believed to cause muscle loss [53, 54], in recent studies, the activation of proteolytic systems in muscle immobilization has also become of great interest [55, 56, 57]. Up-regulation of autophagy and UPS have been implicated in several models of heart and skeletal muscle wasting [58].

Later work has shown a sustained autophagy as well as an activation of UPS after nerve transection [59]. However, while a lot of work has been done on nerve transection, less is known about CCI to the sciatic nerve. Here, we report that the hyperactivation of autophagy and UPS has occurred after CCI. We found that in the skeletal muscle of the damaged hindlimbs, autophagy was associated with increases in Beclin-1, LC3B, and p62 accumulation. p62 protein has a main role in recognition of ubiquitinylated proteins or depolarized mitochondria during selective autophagy; interestingly, it has been described that p62 can also deliver ubiquitinylated cargos to the proteasome [60, 61]. Looking for proteins that play a regulatory role in activation of signalling cascades related to muscle atrophy, TRAF-6, might potentially be an upstream regulator for the activation of pathways involved in loss of muscle proteins in conditions of wasting [15]. TRAF-6 expression is increased in several models of muscle atrophy, including fasting and cancer, leading to downstream activation of major catabolic pathways in skeletal muscle, including autophagy [15, 22]. In accordance with these reports, in the GC CCI model we found an increase of the TRAF-6 gene expression and increased high levels of TRAF-6 protein. Moreover, the protein content of E3 ubiquitin ligase, atrogin-1, up-regulated in the denervated muscle [62], was also up-regulated in the CCI model in our study underlying common pathways of protein degradation in different models of muscle wasting [63]. The gene expression of atrogin-1 evaluated by PCR analysis was found to be upregulated in the GC muscles of the muscle atrophy models induced by both starvation and denervation [64, 65] and this is also confirmed in our model of atrophy induced by ligation of the sciatic nerve. Moreover, the protein content of E3 ubiquitin ligase, atrogin-1, up-regulated in the denervated muscle [62], was also up-regulated in the CCI model in our study underlying common pathways of protein degradation in different models of muscle wasting [63]. Skeletal muscle regeneration is attributed to satellite cells, muscle stem cells resident beneath the basal lamina that surround each myofiber [66, 67]. Pax-7 protein is known to be expressed in quiescent satellite cells, maintained during the progression from quiescence to activation and proliferation, and is then lost during differentiation. We reported that in GC of injured hindlimb, the levels of Pax-7 were sustained 28 after chronic constriction injury. Our findings support that differentiation is impaired in CCI and that such impairment could be a contributor in wasting [68].

Bone mass and skeletal muscle mass are controlled by several factors such as genetics, diet, growth factors and mechanical stimuli. Increased mechanical loading of the musculoskeletal system stimulates an increase in the mass and strength of skeletal muscle and bone, whereas reduced mechanical loading and disuse rapidly promote a decrease in musculoskeletal mass and strength which could lead to muscle atrophy and osteoporosis [69, 70]. Weight-bearing bones are particularly sensitive to the absence of mechanical load, with the proximal femur and tibia exhibiting ∼5% and 23% reductions in bone mineral density following 3 and 6 months of disuse, respectively [71, 72]. Here, we showed that osteoporosis occurs in the ipsilateral tibial bone in rats with sciatic nerve ligation. An experimental study on mononeuropathy in rat described changes in BMC and BMD in the ipsilateral tibial bone [73]. We extended this previous report analyzing new parameters. In our study, at weeks 4 after surgery, many parameters indicating bone frailty, such as bone mineral density (BMD), bone volume fraction (BV/TV), bone surface density (BS/TV), trabecular number (Tb.N), connectivity density, bone perimeter (B.Pm) of the tibial bone on the ipsilateral hindlimb side were lower than the contralateral tibial bone, whereas the

structure model index (SMI) was higher on the contralateral side bone. Furthermore, we analyzed some osteoporosis-related markers, such as ALP, OPG, RUNX2, RANKL and TRAF-6, however in the ipsilateral femurs of animals subjected to CCI, we observed only a significative increase of TRAF-6 gene expression. This gene could cause an alteration of the physiological bone remodelling [74]. In fact, the deletion of TRAF-6 is associated with an increase in the number of osteoblasts and a reduction of osteoclasts, as well as an increase in bone mineral density [75]. Two possible mechanisms may be involved in the pathogenesis of the osteoporosis/osteopenia associated with CCI. One is the partial immobilization of the hindlimb. Previous reports showed that, in mice with cast immobilization osteopenia developed within 10–21 days, with diminished BMC, decreased dry bone mass, bone mineral density and metaphyseal bone volume [76, 77, 78, 79]. The osteopathy seen in mice with cast immobilization is quite similar to the osteopathy that we report in this study. In addition to immobilization, the nerve injury could also be directly responsible for osteopathy. Bone is densely innervated to the periosteum of the metaphyseal region and the primary afferent axons that innervate the bone contain neuropeptides [80]. If such neuropeptides are released from the nerve and affect bone metabolism, osteoporosis could be related to their activity. Loose ligation of the sciatic nerve in rats induced an inflammatory response in the ipsilateral hind paw, hence an increase in myeloperoxidase activity in the muscle, as well as increased skin blood flow and oedema in the ipsilateral hind paw on day 4 after surgery have already been described. Neuropeptides, such as substance-P, released from nerve terminals in the injured axons, caused the increased synthesis and release of monocyte derived cytokines [81, 82]. These cytokines can also induce osteoclastogenesis [83] and, therefore, may subsequently cause osteoporosis.

Although further experiments are needed to better characterize the mechanisms underlying the muscle atrophy and osteopathy, chronic sciatic nerve constriction appears a valid approach to study the muscle-bone crosstalk, and the identification of new and more effective strategies to prevent osteosarcopenia.

Abbreviations

ALP Alkaline Phosphatase

fbx32 Atrogin-1

BMC Bone Mineral Content

BMD Bone Mineral Density

B.Pm Bone Perimeter

BV/TV Bone Volume Fraction

CCI Chronic Constriction Injury

COPD Chronic Obstructive Pulmonary Disease

CI Confidence Interval

Conn.D Connectivity Density

CSA Cross-sectional Area

EDL Extensor Digitalis Longus Muscle

GC Gastrocnemius

H&E Hematoxylin and Eosin

LC3B-I Light Chain 3B Isoform I

MRI Magnetic Resonance Imaging

Micro-CT Micro-Computed Tomography

OPG Osteoprotegerin

Pax-7 Paired Box 7

qRT-PCR Quantitative Real Time PCR

RANKL Receptor Activator of Nuclear Factor Kappa Beta

RUNX2 Runt-related Transcription Factor 2

SMI Structure Model Index

Ct Threshold Cycle

TRAF-6 TNF Receptor-Associated Factor 6

Tb.N Trabecular Number

Tb.Sp Trabecular Separation

Tb.Th Trabecular Thickness

TBS Tris Buffered Saline

UPS Ubiquitin-Proteasome System

Declarations

Authors' contributions

V.M., M.G. and Vincenzo Musolino conceptualized and designed the study. F.B., M.S., S.N., S.I., L.A.G., F.L., L.G. performed the intervention. F.B. wrote the manuscript. A.C, F.B., and Vincenzo Musolino analyzed the data and interpretated analysis. S.N. performed histological analysis. S.N., S.R. and A.C. performed magnetic resonance imaging (MRI) and Micro-CT studies. I.B., F.B., C.C., C.R., L.G., R.M., J.M., E.P., F.S., S.M., M.S., F.C., R.C., C.M. performed experiments. All authors reviewed the manuscript.

Acknowledgements

Not applicable

Funding

This research was funded by PON-MIUR 03PE000_78_1 and PONMIUR 03PE000_78_2. POR Calabria FESR FSE 2014–2020 Asse 12-Azioni 10.5.6 e 10.5.12.

Availability of data and materials

The datasets generated or analyzed during the current study are available from the corresponding author upon reasonable request. Materials used in this study are commercially available.

Ethics approval and consent to participate

All the experimental procedures were performed according to protocols approved by the Animal Care of University Magna Graecia of Catanzaro. The experimental procedures were carried out in compliance with the ARRIVE guidelines. All experiments were performed in accordance with the European Commission guidelines (Directive 2010/63/EU) for the animals used for scientific purposes.

Consent for publication

Not applicable.

Competing interests

The authors declare no competing interests.

References

1. Argiles JM, Campos N, Lopez-Pedrosa JM, Rueda R, Rodriguez-Manas L. Skeletal Muscle Regulates Metabolism via Interorgan Crosstalk: Roles in Health and Disease. J Am Med Dir Assoc. 2016;17(9):789–96.
2. Chargi N, Bril SI, Swartz JE, Wegner I, Willems SM, de Bree R. Skeletal muscle mass is an imaging biomarker for decreased survival in patients with oropharyngeal squamous cell carcinoma. Oral Oncol. 2020;101:104519.

3. von Haehling S, Garfias Macedo T, Valentova M, Anker MS, Ebner N, Bekfani T, et al. Muscle wasting as an independent predictor of survival in patients with chronic heart failure. J Cachexia Sarcopenia Muscle. 2020;11(5):1242–9.
4. Tieland M, Trouwborst I, Clark BC. Skeletal muscle performance and ageing. J Cachexia Sarcopenia Muscle. 2018;9(1):3–19.
5. Ebert SM, Al-Zougbi A, Bodine SC, Adams CM. Skeletal Muscle Atrophy: Discovery of Mechanisms and Potential Therapies. Physiology (Bethesda). 2019;34(4):232–9.
6. Calvani R, Miccheli A, Landi F, Bossola M, Cesari M, Leeuwenburgh C, et al. Current nutritional recommendations and novel dietary strategies to manage sarcopenia. J Frailty Aging. 2013;2(1):38–53.
7. Shen L, Meng X, Zhang Z, Wang T. Physical Exercise for Muscle Atrophy. Adv Exp Med Biol. 2018;1088:529–45.
8. Kirk B, Zanker J, Duque G. Osteosarcopenia: epidemiology, diagnosis, and treatment-facts and numbers. J Cachexia Sarcopenia Muscle. 2020;11(3):609–18.
9. Ramdharry G. Peripheral nerve disease. Handb Clin Neurol. 2018;159:403–15.
10. Jones PE, Meyer RM, Faillace WJ, Landau ME, Smith JK, McKay PL, et al. Combat Injury of the Sciatic Nerve - An Institutional Experience. Mil Med. 2018;183(9–10):e434-e41.
11. Welch JA. Peripheral nerve injury. Semin Vet Med Surg Small Anim. 1996;11(4):273–84.
12. Bennett GJ, Xie YK. A peripheral mononeuropathy in rat that produces disorders of pain sensation like those seen in man. Pain. 1988;33(1):87–107.
13. Langer HT, Senden JMG, Gijsen AP, Kempa S, van Loon LJC, Spuler S. Muscle Atrophy Due to Nerve Damage Is Accompanied by Elevated Myofibrillar Protein Synthesis Rates. Front Physiol. 2018;9:1220.
14. Langer HT, Afzal S, Kempa S, Spuler S. Nerve damage induced skeletal muscle atrophy is associated with increased accumulation of intramuscular glucose and polyol pathway intermediates. Sci Rep. 2020;10(1):1908.
15. Kumar A, Bhatnagar S, Paul PK. TWEAK and TRAF-6 regulate skeletal muscle atrophy. Curr Opin Clin Nutr Metab Care. 2012;15(3):233–9.
16. Vainshtein A, Sandri M. Signaling Pathways That Control Muscle Mass. Int J Mol Sci. 2020;21(13).
17. Guadagnin E, Mazala D, Chen YW. STAT3 in Skeletal Muscle Function and Disorders. Int J Mol Sci. 2018;19(8).
18. Anthony TG. Mechanisms of protein balance in skeletal muscle. Domest Anim Endocrinol. 2016;56 Suppl:S23-32.
19. Gordon BS, Kelleher AR, Kimball SR. Regulation of muscle protein synthesis and the effects of catabolic states. Int J Biochem Cell Biol. 2013;45(10):2147–57.
20. Musolino V, Palus S, Tschirner A, Drescher C, Gliozzi M, Carresi C, et al. Megestrol acetate improves cardiac function in a model of cancer cachexia-induced cardiomyopathy by autophagic modulation.

J Cachexia Sarcopenia Muscle. 2016;7(5):555–66.

21. Paul PK, Bhatnagar S, Mishra V, Srivastava S, Darnay BG, Choi Y, et al. The E3 ubiquitin ligase TRAF-6 intercedes in starvation-induced skeletal muscle atrophy through multiple mechanisms. Mol Cell Biol. 2012;32(7):1248–59.
22. Paul PK, Kumar A. TRAF-6 coordinates the activation of autophagy and ubiquitin-proteasome systems in atrophying skeletal muscle. Autophagy. 2011;7(5):555–6.
23. Schiaffino S, Dyar KA, Ciciliot S, Blaauw B, Sandri M. Mechanisms regulating skeletal muscle growth and atrophy. FEBS J. 2013;280(17):4294–314.
24. Song JY, Pineault KM, Wellik DM. Development, repair, and regeneration of the limb musculoskeletal system. Curr Top Dev Biol. 2019;132:451–86.
25. Manas-Garcia L, Guitart M, Duran X, Barreiro E. Satellite Cells and Markers of Muscle Regeneration during Unloading and Reloading: Effects of Treatment with Resveratrol and Curcumin. Nutrients. 2020;12(6).
26. McKenna CF, Fry CS. Altered satellite cell dynamics accompany skeletal muscle atrophy during chronic illness, disuse, and aging. Curr Opin Clin Nutr Metab Care. 2017;20(6):447–52.
27. Bettis T, Kim BJ, Hamrick MW. Impact of muscle atrophy on bone metabolism and bone strength: implications for muscle-bone crosstalk with aging and disuse. Osteoporos Int. 2018;29(8):1713–20.
28. Bateman TA, Dunstan CR, Lacey DL, Ferguson VL, Ayers RA, Simske SJ. Osteoprotegerin ameliorates sciatic nerve crush induced bone loss. J Orthop Res. 2001;19(4):518–23.
29. Suyama H, Moriwaki K, Niida S, Maehara Y, Kawamoto M, Yuge O. Osteoporosis following chronic constriction injury of sciatic nerve in rats. J Bone Miner Metab. 2002;20(2):91–7.
30. Strotmeyer ES, Cauley JA, Schwartz AV, de Rekeneire N, Resnick HE, Zmuda JM, et al. Reduced peripheral nerve function is related to lower hip BMD and calcaneal QUS in older white and black adults: the Health, Aging, and Body Composition Study. J Bone Miner Res. 2006;21(11):1803–10.
31. Musolino V, Palus S, Latouche C, Gliozzi M, Bosco F, Scarano F, et al. Cardiac expression of neutrophil gelatinase-associated lipocalin in a model of cancer cachexia-induced cardiomyopathy. ESC Heart Fail. 2019;6(1):89–97.
32. Greene. Anatomy of the Rat: Hafner Publishing Company; 1963.
33. Zhang J, Zhang G, Morrison B, Mori S, Sheikh KA. Magnetic resonance imaging of mouse skeletal muscle to measure denervation atrophy. Exp Neurol. 2008;212(2):448–57.
34. Maurotti S, Russo C, Musolino V, Nucera S, Gliozzi M, Scicchitano M, et al. Effects of C-Peptide Replacement Therapy on Bone Microarchitecture Parameters in Streptozotocin-Diabetic Rats. Calcif Tissue Int. 2020;107(3):266–80.
35. Wilhelm J, Pingoud A. Real-time polymerase chain reaction. Chembiochem. 2003;4(11):1120–8.
36. Fonseca-Rodrigues D, Amorim D, Almeida A, Pinto-Ribeiro F. Emotional and cognitive impairments in the peripheral nerve chronic constriction injury model (CCI) of neuropathic pain: A systematic review. Behav Brain Res. 2021;399:113008.

37. Matias Junior I, Medeiros P, de Freita RL, Vicente-Cesar H, Ferreira Junior JR, Machado HR, et al. Effective Parameters for Gait Analysis in Experimental Models for Evaluating Peripheral Nerve Injuries in Rats. Neurospine. 2019;16(2):305–16.
38. Austin PJ, Wu A, Moalem-Taylor G. Chronic constriction of the sciatic nerve and pain hypersensitivity testing in rats. J Vis Exp. 2012(61).
39. Ilari S, Dagostino C, Malafoglia V, Lauro F, Giancotti LA, Spila A, et al. Protective Effect of Antioxidants in Nitric Oxide/COX-2 Interaction during Inflammatory Pain: The Role of Nitration. Antioxidants (Basel). 2020;9(12).
40. Choe MA, Kim KH, An GJ, Lee KS, Heitkemper M. Hindlimb muscle atrophy occurs from peripheral nerve damage in a rat neuropathic pain model. Biol Res Nurs. 2011;13(1):44–54.
41. Leiphart JW, Vasudevan PP, Rajjoub SR, Dominguez LW, Chang J. The effect of acute postoperative pain and chronic neuropathic pain on subsequent weight gain in the rat. J Neurosurg. 2010;112(4):780–3.
42. Richner M, Bjerrum OJ, Nykjaer A, Vaegter CB. The spared nerve injury (SNI) model of induced mechanical allodynia in mice. J Vis Exp. 2011(54).
43. Beehler BC, Sleph PG, Benmassaoud L, Grover GJ. Reduction of skeletal muscle atrophy by a proteasome inhibitor in a rat model of denervation. Exp Biol Med (Maywood). 2006;231(3):335–41.
44. Daemen MA, Kurvers HA, Bullens PH, Slaaf DW, Freling G, Kitslaar PJ, et al. Motor denervation induces altered muscle fibre type densities and atrophy in a rat model of neuropathic pain. Neurosci Lett. 1998;247(2–3):204–8.
45. Yang X, Xue P, Chen H, Yuan M, Kang Y, Duscher D, et al. Denervation drives skeletal muscle atrophy and induces mitochondrial dysfunction, mitophagy and apoptosis via miR-142a-5p/MFN1 axis. Theranostics. 2020;10(3):1415–32.
46. Arnold WD, Kassar D, Kissel JT. Spinal muscular atrophy: diagnosis and management in a new therapeutic era. Muscle Nerve. 2015;51(2):157–67.
47. Wu H, Li L, Su X. Vagus nerve through alpha7 nAChR modulates lung infection and inflammation: models, cells, and signals. Biomed Res Int. 2014;2014:283525.
48. Zhao YX, He W, Jing XH, Liu JL, Rong PJ, Ben H, et al. Transcutaneous auricular vagus nerve stimulation protects endotoxemic rat from lipopolysaccharide-induced inflammation. Evid Based Complement Alternat Med. 2012;2012:627023.
49. Leterme D, Tyc F. Re-innervation and recovery of rat soleus muscle and motor unit function after nerve crush. Exp Physiol. 2004;89(4):353–61.
50. Shimkus KL, Jefferson LS, Gordon BS, Kimball SR. Repressors of mTORC1 act to blunt the anabolic response to feeding in the soleus muscle of a cast-immobilized mouse hindlimb. Physiol Rep. 2018;6(20):e13891.
51. Jaspers SR, Tischler ME. Atrophy and growth failure of rat hindlimb muscles in tail-cast suspension. J Appl Physiol Respir Environ Exerc Physiol. 1984;57(5):1472–9.

52. Bederman IR, Lai N, Shuster J, Henderson L, Ewart S, Cabrera ME. Chronic hindlimb suspension unloading markedly decreases turnover rates of skeletal and cardiac muscle proteins and adipose tissue triglycerides. J Appl Physiol (1985). 2015;119(1):16–26.
53. Wall BT, Snijders T, Senden JM, Ottenbros CL, Gijsen AP, Verdijk LB, et al. Disuse impairs the muscle protein synthetic response to protein ingestion in healthy men. J Clin Endocrinol Metab. 2013;98(12):4872–81.
54. Phillips SM. A brief review of critical processes in exercise-induced muscular hypertrophy. Sports Med. 2014;44 Suppl 1:S71-7.
55. Talbert EE, Smuder AJ, Min K, Kwon OS, Szeto HH, Powers SK. Immobilization-induced activation of key proteolytic systems in skeletal muscles is prevented by a mitochondria-targeted antioxidant. J Appl Physiol (1985). 2013;115(4):529–38.
56. Ji LL, Yeo D. Mitochondrial dysregulation and muscle disuse atrophy. F1000Res. 2019;8.
57. Hyatt H, Deminice R, Yoshihara T, Powers SK. Mitochondrial dysfunction induces muscle atrophy during prolonged inactivity: A review of the causes and effects. Arch Biochem Biophys. 2019;662:49–60.
58. Cohen S, Nathan JA, Goldberg AL. Muscle wasting in disease: molecular mechanisms and promising therapies. Nat Rev Drug Discov. 2015;14(1):58–74.
59. Joshi SK, Kim HT, Feeley BT, Liu X. Differential ubiquitin-proteasome and autophagy signaling following rotator cuff tears and suprascapular nerve injury. J Orthop Res. 2014;32(1):138–44.
60. Johansen T, Lamark T. Selective autophagy mediated by autophagic adapter proteins. Autophagy. 2011;7(3):279–96.
61. Kirkin V, McEwan DG, Novak I, Dikic I. A role for ubiquitin in selective autophagy. Mol Cell. 2009;34(3):259–69.
62. Hanai J, Cao P, Tanksale P, Imamura S, Koshimizu E, Zhao J, et al. The muscle-specific ubiquitin ligase atrogin-1/MAFbx mediates statin-induced muscle toxicity. J Clin Invest. 2007;117(12):3940–51.
63. Bialek P, Morris C, Parkington J, St Andre M, Owens J, Yaworsky P, et al. Distinct protein degradation profiles are induced by different disuse models of skeletal muscle atrophy. Physiol Genomics. 2011;43(19):1075–86.
64. Bodine SC, Stitt TN, Gonzalez M, Kline WO, Stover GL, Bauerlein R, et al. Akt/mTOR pathway is a crucial regulator of skeletal muscle hypertrophy and can prevent muscle atrophy in vivo. Nat Cell Biol. 2001;3(11):1014–9.
65. Gomes MD, Lecker SH, Jagoe RT, Navon A, Goldberg AL. Atrogin-1, a muscle-specific F-box protein highly expressed during muscle atrophy. Proc Natl Acad Sci U S A. 2001;98(25):14440–5.
66. Dumont NA, Bentzinger CF, Sincennes MC, Rudnicki MA. Satellite Cells and Skeletal Muscle Regeneration. Compr Physiol. 2015;5(3):1027–59.

67. Song T, Sadayappan S. Featured characteristics and pivotal roles of satellite cells in skeletal muscle regeneration. J Muscle Res Cell Motil. 2020;41(4):341–53.
68. Viguie CA, Lu DX, Huang SK, Rengen H, Carlson BM. Quantitative study of the effects of long-term denervation on the extensor digitorum longus muscle of the rat. Anat Rec. 1997;248(3):346–54.
69. Reilly BD, Franklin CE. Prevention of muscle wasting and osteoporosis: the value of examining novel animal models. J Exp Biol. 2016;219(Pt 17):2582–95.
70. Kaji H. Interaction between Muscle and Bone. J Bone Metab. 2014;21(1):29–40.
71. Watanabe Y. An assessment of osteoporosis in stroke patients on rehabilitation admission. Int J Rehabil Res. 2004;27(2):163–6.
72. Young DR, Niklowitz WJ, Steele CR. Tibial changes in experimental disuse osteoporosis in the monkey. Calcif Tissue Int. 1983;35(3):304–8.
73. Suyama H, Kawamoto M, Gaus S, Yuge O. Effect of etodolac, a COX-2 inhibitor, on neuropathic pain in a rat model. Brain Res. 2004;1010(1–2):144–50.
74. Kadono Y, Okada F, Perchonock C, Jang HD, Lee SY, Kim N, et al. Strength of TRAF-6 signalling determines osteoclastogenesis. EMBO Rep. 2005;6(2):171–6.
75. Oya A, Katsuyama E, Morita M, Sato Y, Kobayashi T, Miyamoto K, et al. Tumor necrosis factor receptor-associated factor 6 is required to inhibit foreign body giant cell formation and activate osteoclasts under inflammatory and infectious conditions. J Bone Miner Metab. 2018;36(6):679–90.
76. Lodberg A, Vegger JB, Jensen MV, Larsen CM, Thomsen JS, Bruel A. Immobilization induced osteopenia is strain specific in mice. Bone Rep. 2015;2:59–67.
77. Hott M, Deloffre P, Tsouderos Y, Marie PJ. S12911-2 reduces bone loss induced by short-term immobilization in rats. Bone. 2003;33(1):115–23.
78. Rantakokko J, Uusitalo H, Jamsa T, Tuukkanen J, Aro HT, Vuorio E. Expression profiles of mRNAs for osteoblast and osteoclast proteins as indicators of bone loss in mouse immobilization osteopenia model. J Bone Miner Res. 1999;14(11):1934–42.
79. Weinreb M, Rodan GA, Thompson DD. Osteopenia in the immobilized rat hind limb is associated with increased bone resorption and decreased bone formation. Bone. 1989;10(3):187–94.
80. Garcia-Castellano JM, Diaz-Herrera P, Morcuende JA. Is bone a target-tissue for the nervous system? New advances on the understanding of their interactions. Iowa Orthop J. 2000;20:49–58.
81. Ellis A, Bennett DL. Neuroinflammation and the generation of neuropathic pain. Br J Anaesth. 2013;111(1):26–37.
82. Suvas S. Role of Substance P Neuropeptide in Inflammation, Wound Healing, and Tissue Homeostasis. J Immunol. 2017;199(5):1543–52.
83. Amarasekara DS, Yun H, Kim S, Lee N, Kim H, Rho J. Regulation of Osteoclast Differentiation by Cytokine Networks. Immune Netw. 2018;18(1):e8.

Figures

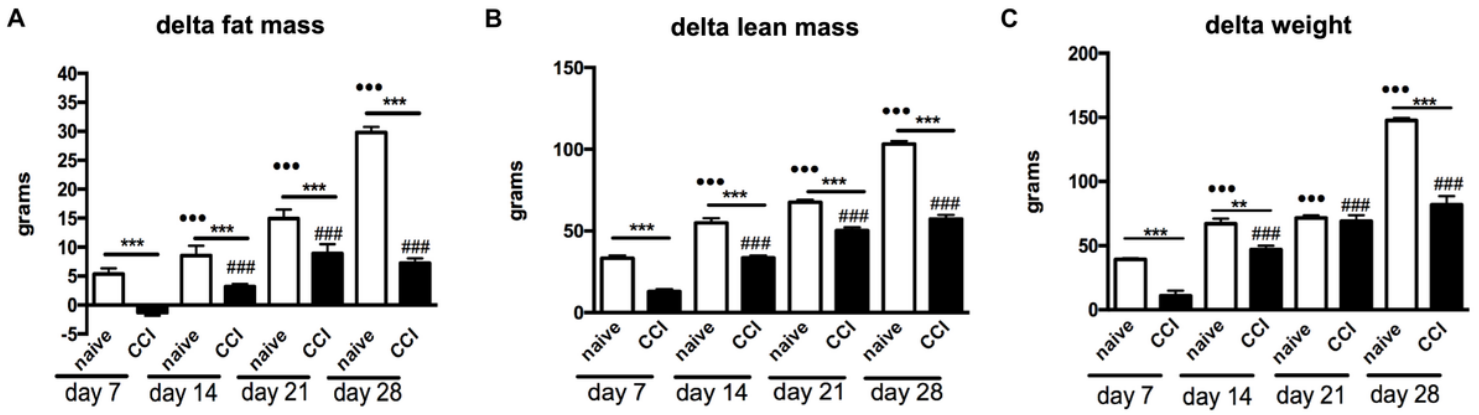

Figure 1

Effects of CCI of the sciatic nerve on weight and body composition. The variations of body weight **(A)**, fat mass **(B)**, and lean mass **(C)** are presented as the absolute difference between baseline values and the values observed every seven days after the intervention. The results are expressed as mean ± S.E.M. •••: p<0.001 vs Naive day 7; ###: p<0.001 vs CCI day 7; **: p <0.01 at 14 days; ***: p<0.001 at 7 and 28 days.

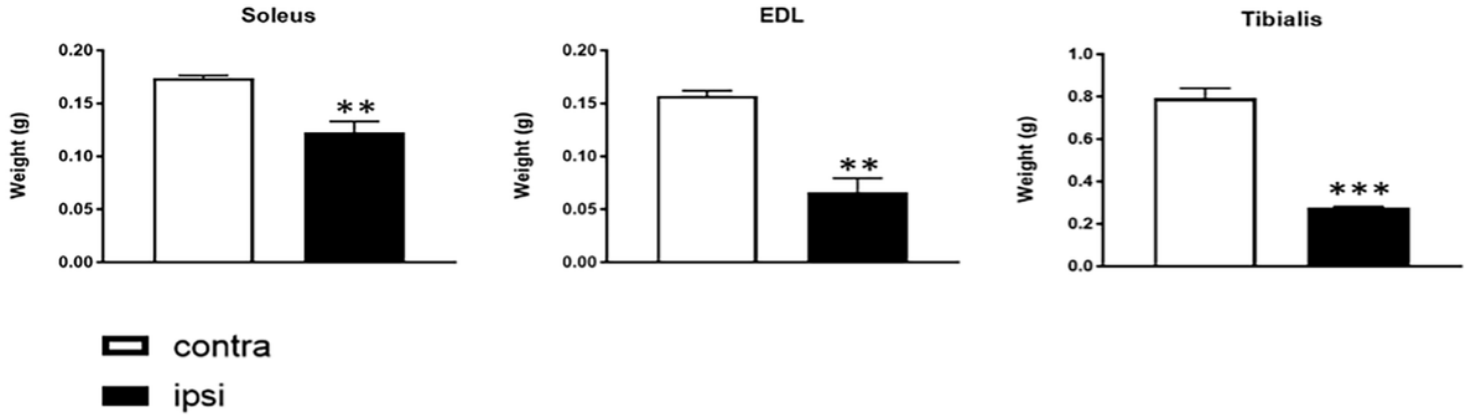

Figure 2

Skeletal muscles weight at the end of the study. The results are expressed as mean ± S.E.M. **: p<0.01, ***: p<0.001 vs contralateral.

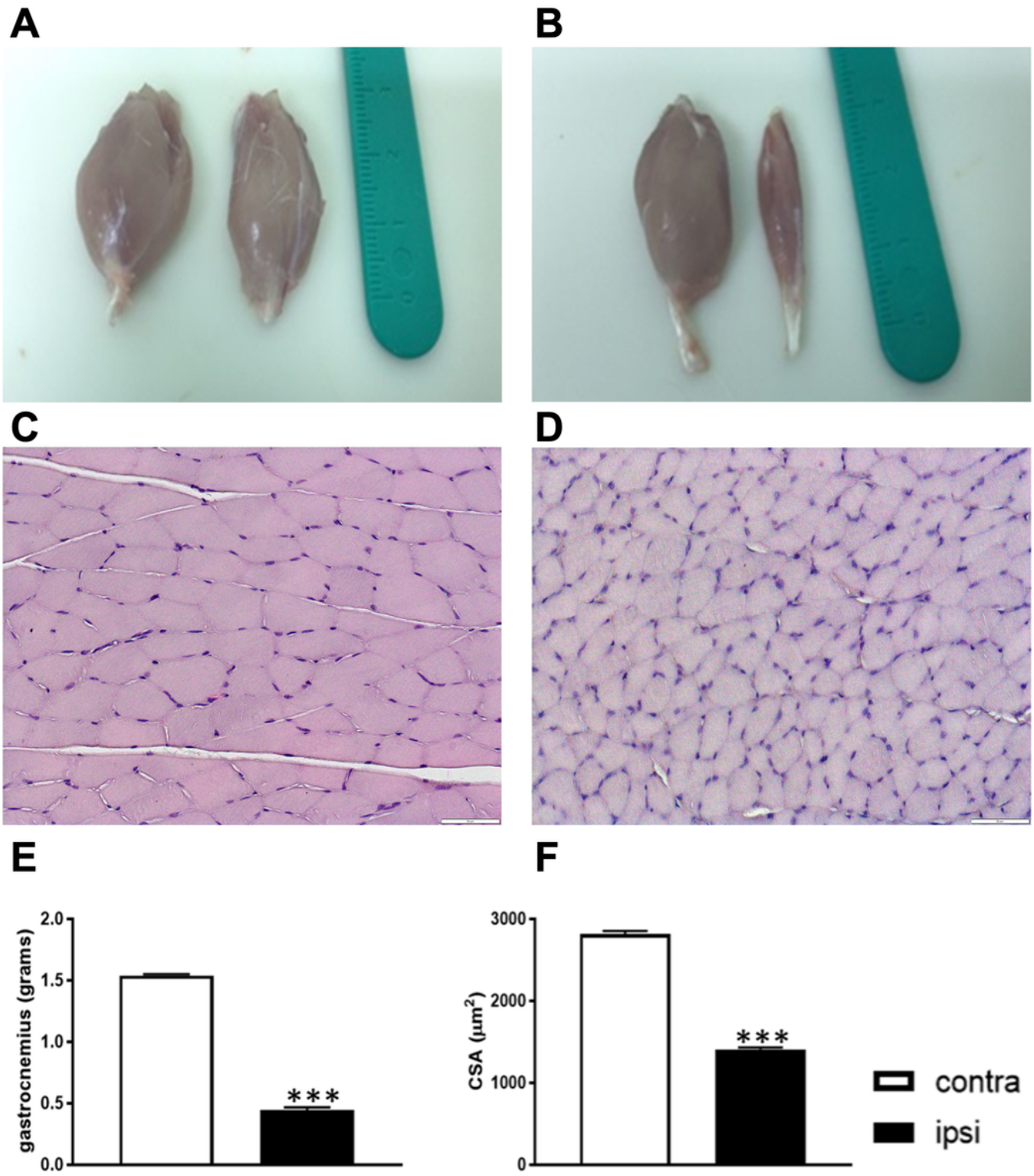

Figure 3

Gastrocnemius muscles of rats subjected to CCI exhibit an atrophic phenotype at day 28. (Top) Representative photos of GC muscles of a naïve animal **(A)** and a CCI animal **(B)** explanted at day 28 of the experiment. **(Middle)** Representative haematoxylin and eosin (H&E) staining image of contralateral **(C)** and ipsilateral **(D)** GC muscle; Scale bar: 50 µm. **(Bottom)** GC weight of the contralateral injured ipsilateral hindlimb is lower than contralateral GC weight at day 28 **(E)**; Cross sectional area (CSA) of

muscle fibers decreased in ipsilateral GC compared to contralateral side **(F)**. The results are expressed as mean ± S.E.M. ***: p<0.001 vs contralateral.

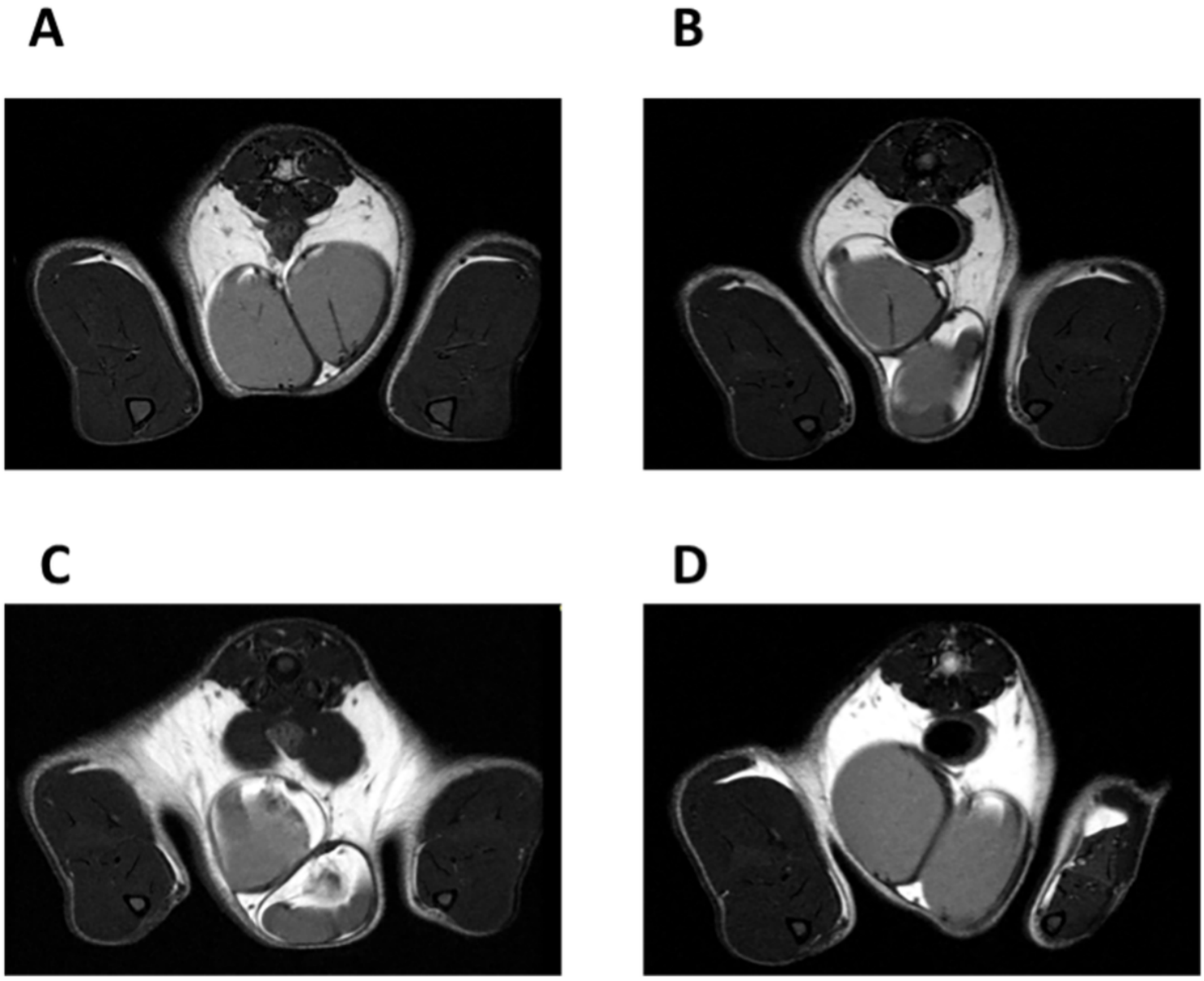

Figure 4

Representative axial T2_turboRARE weighted images with fat suppression of rat hindlimbs. Naïve rat at day 0 **(A)** and at day 28 **(B)**; CCI rat at day 0 **(C)** and at day 28 **(D)**.

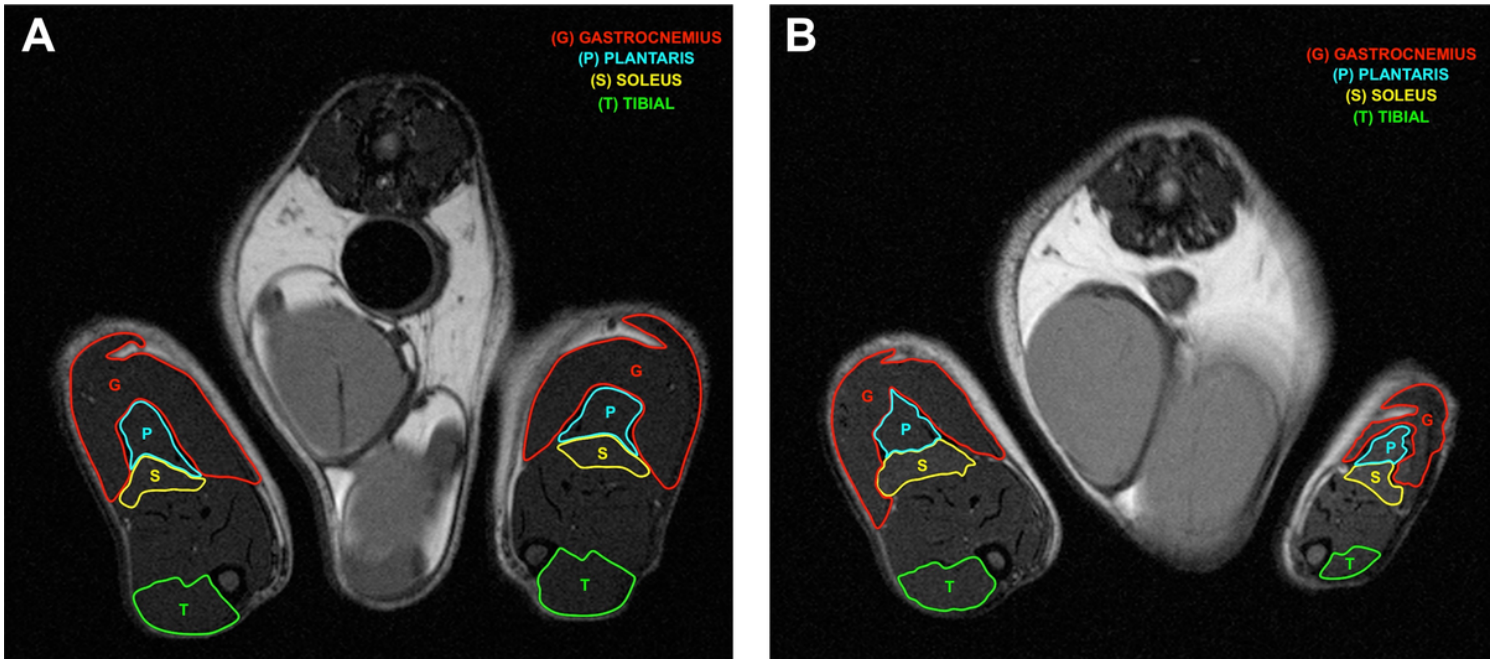

Figure 5

Manual segmentations of individual muscles in axial T2_weighted images with fat suppression of rat hindlimbs. Naïve rat **(A)** and CCI rat **(B)** at day 28.

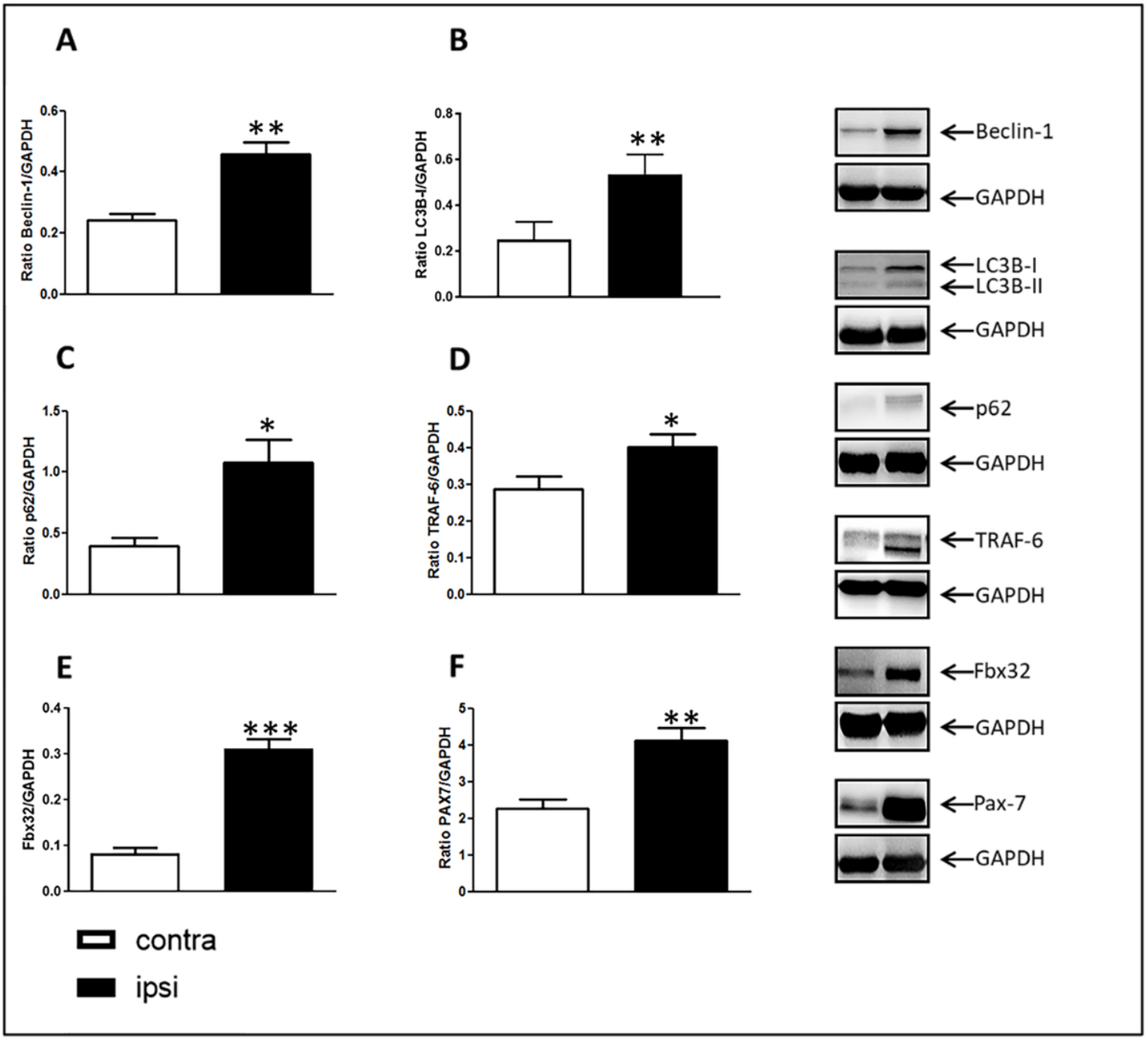

Figure 6

Western blotting images and densitometric analysis of markers analysed in the gastrocnemius muscle at day 28. Expression in injured ipsilateral GC and contralateral muscle of Beclin-1 **(A)**, Autophagic marker LC3 **(B)**, p62 **(C)**, TRAF-6 **(D)**, Ubiquitin-protein ligase **(E)**. Densitometric analysis of Pax-7 expression levels **(F)**. The results are expressed as mean ± S.E.M. *: p<0.05, **: p<0.01, ***: p<0.001 vs contralateral.

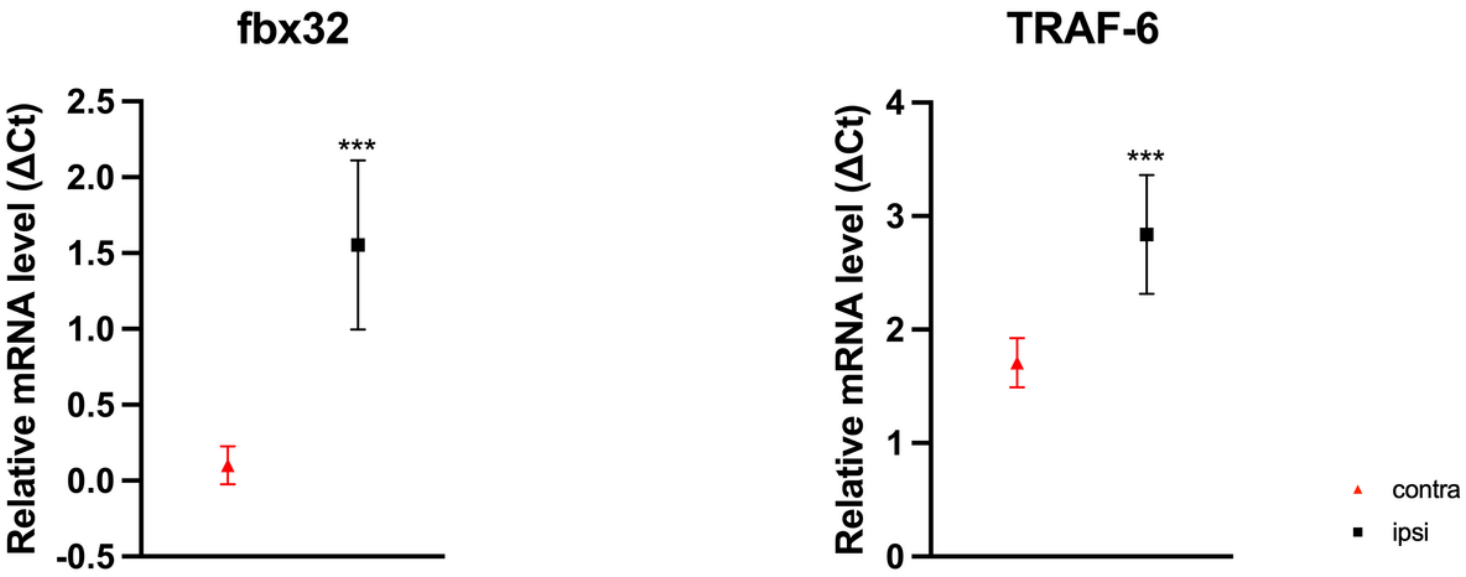

Figure 7

Results of real-time PCR. The results are plotted as relative mRNA levels (ΔCt) and presented as mean and their 95% confidence intervals (CI). ***: $p<0.001$ vs contralateral.

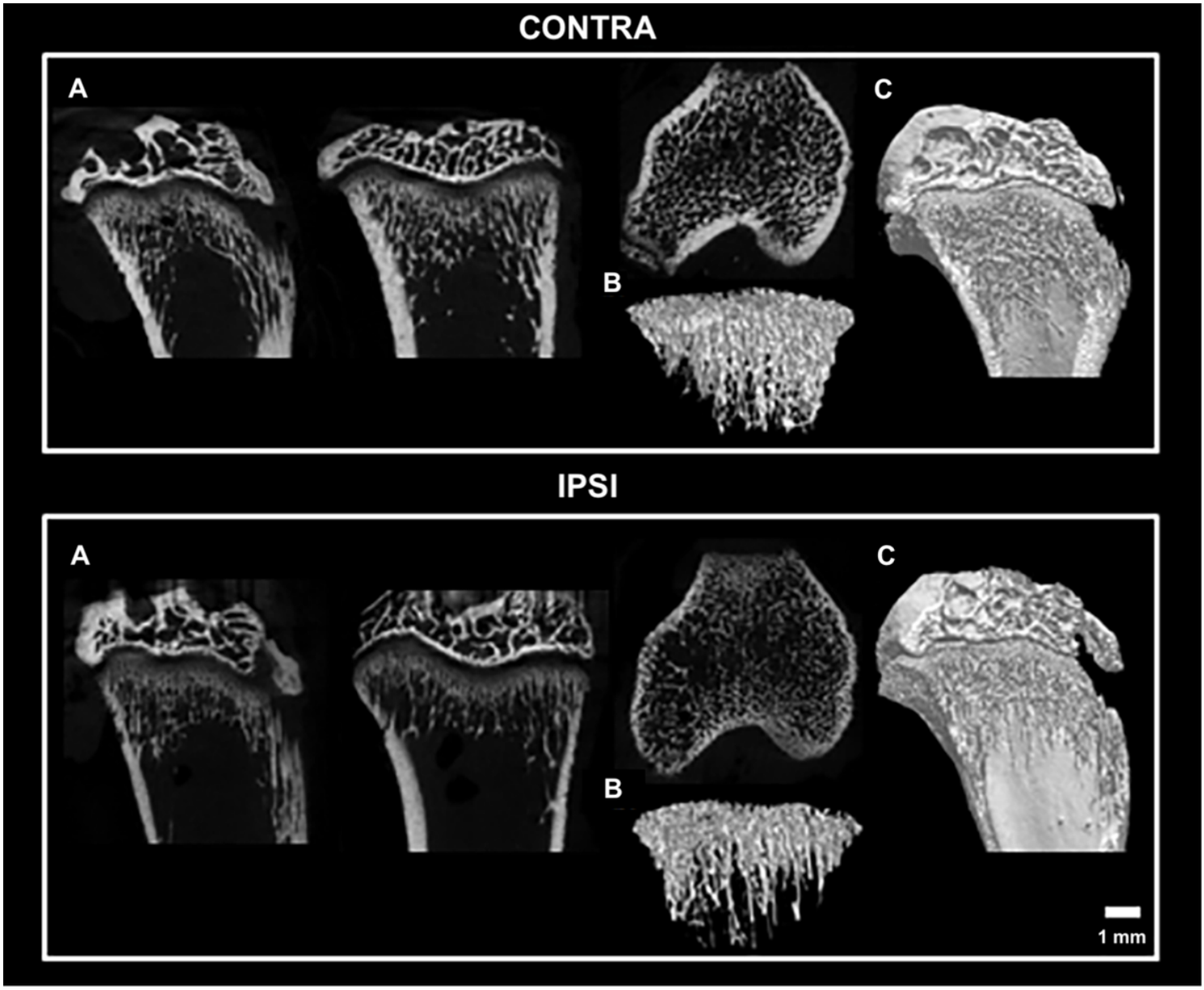

Figure 8

Representative micro-CT images showing trabecular architecture of the distal femur. (A) Coronal, sagittal and trans-axial sections; **(B)** Three-dimensional trabecular architecture; **(C)** Three-dimensional architecture of the distal femur in coronal view. Contralateral **(Top)**, Ipsilateral **(Bottom)**. Scale bar: 1mm.

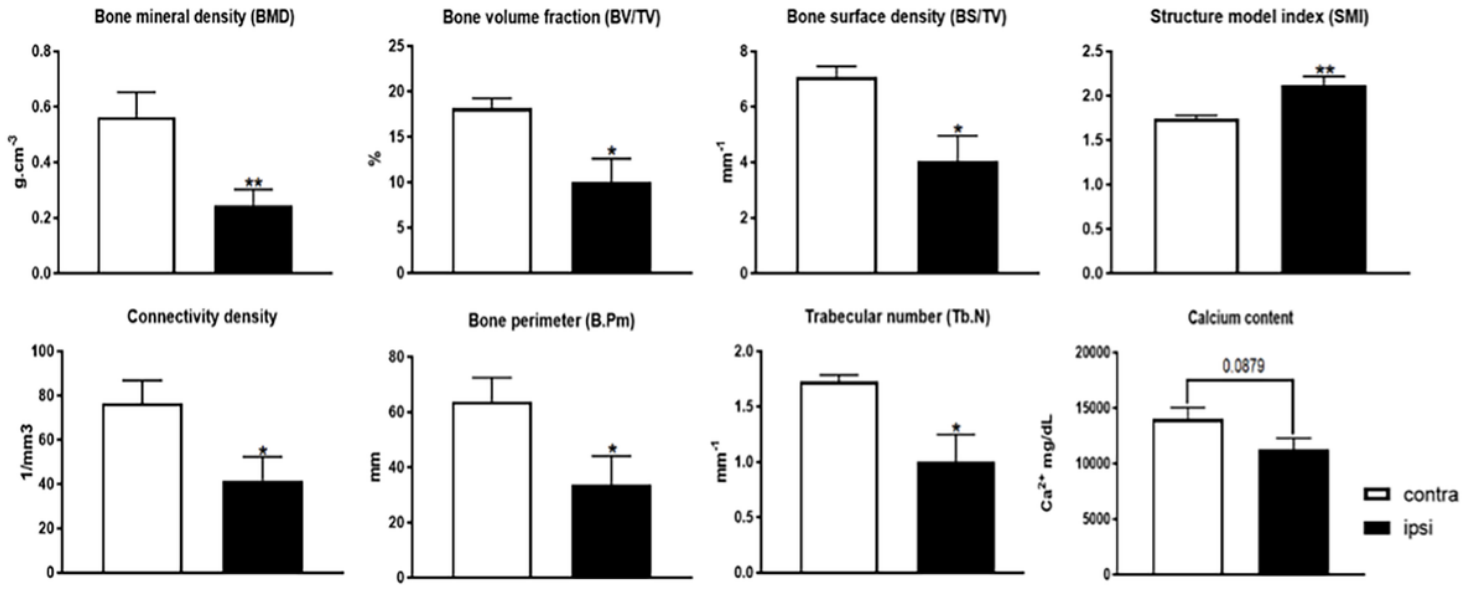

Figure 9

Bone structural parameters and calcium 4 weeks after the surgery. The results are expressed as mean ± S.E.M. *: p<0.05, **: p<0.01 vs contralateral.

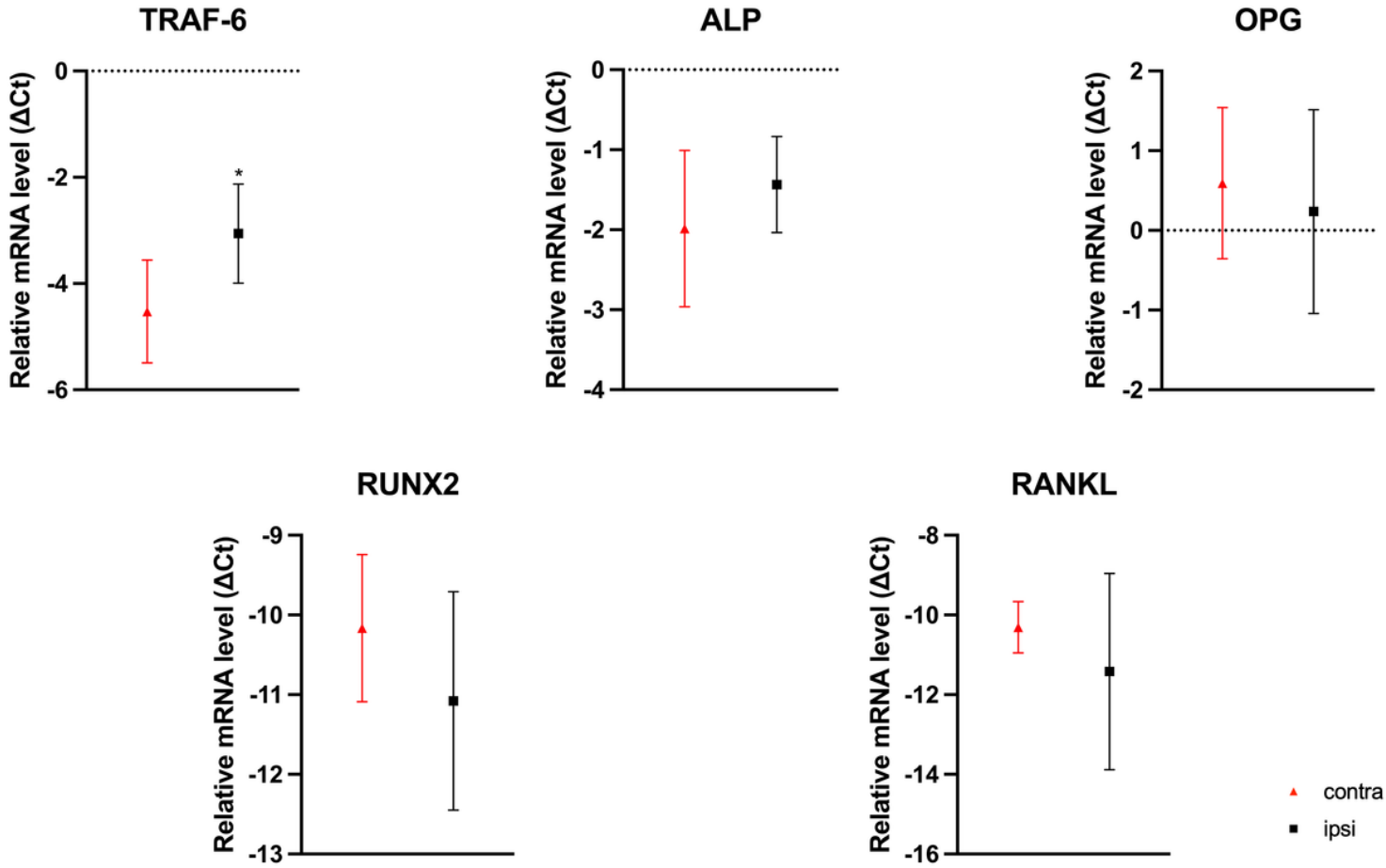

Figure 10

Results of real-time quantitative PCR in femurs. The results are plotted as relative mRNA levels (ΔCt) and presented as mean and their 95% confidence intervals (CI). *: $p<0.05$ vs contralateral.